Dissolved Gas Analysis of Insulating Transformer Oil Using Optical Fiber

Alan B. Overby

Thesis submitted to the faculty of the Virginia Polytechnic Institute and State University in partial fulfillment of the requirements for the degree of

Master of Science
in
Electrical Engineering

Anbo Wang, Committee Chair
Gary R. Pickrell
Yong Xu

May 14, 2014
Blacksburg, VA

Key words: Optical fiber sensing, Dissolved gas analysis, Hydrogen sensor, Acetylene sensor, Transformer monitoring

Dissolved Gas Analysis of Insulating Transformer Oil Using Optical Fiber

Alan B. Overby

ABSTRACT

The power industry relies on high voltage transformers as the backbone of power distribution networks. High voltage transformers are designed to handle immense electrical loads in hostile environments. Long term placement is desired, however by being under constant heavy load transformers face mechanical, thermal, and electrical stresses which lead to failures of the protection systems in place. The service life of a transformer is often limited by the life time of its insulation system. Insulation failures most often develop from thermal faults, or hotspots, and electrical faults, or partial discharges. Detecting hotspots and partial discharges to predict transformer life times is imperative and much research is focused towards these topics. As these protection systems fail they often generate gas or acoustic signals signifying a problem. Research has already been performed discovering new ways integrate optical fiber sensors into high voltage transformers. This thesis is a continuation of that research by attempting to improve sensor sensitivity for hydrogen and acetylene gasses. Of note is the fabrication of new hydrogen sensing fiber for operation around a larger absorption peak and also the improvement of the acetylene sensor's light source stability. Also detailed is the manufacturing of a field testable prototype and the non-sensitivity testing of several other gasses. The developed sensors are capable but still could be improved with the use of more powerful and stable light sources.

Dedications

First and foremost I want to thank God for guiding me to where I am today and for equipping me with the abilities I have.

I am eternally grateful for my family and friends who have been there at all stages. Their guidance and support made it possible to flourish even in the hardest of times.

I want to thank Dr. Wang for developing a workplace that takes pride in seeking excellence and for being a constant source of guidance, motivation, and encouragement. The Center for Photonics Technology is a place that many consider a second home.

I am truly grateful for the mentorship I have received from Bo Dong and Dorothy Wang. They have each devoted their time and expertise to this project. I am proud to have been part of that team.

Finally, I am especially thankful for the friendship and helpfulness of all my lab mates, especially Li Yu, Di Hu, and Bo Liu who have all contributed effort and know-how to this project. Li Yu, you always gave 100% no matter how late we worked or how fruitless things seemed at the time.

Acknowledgements

This work was sponsored by the Electric Power Research Institute. Their financial support and enthusiasm were greatly appreciated. The Electric Power Research Institute project number that corresponded to this work was 072653

Photos by author, 2014.

Table of Contents

Listing of Figures

Listing of Tables

1 Introduction

1.1 High Voltage Transformer Monitoring Background

The power industry relies on high voltage transformers as the backbone of power distribution networks. These transformers are as common as they are expensive. High voltage transformers are designed to handle immense electrical loads in hostile environments. As such, they require sturdy construction and protection systems which make their construction costs exceptionally expensive. Long term placement is desired, however by being under constant heavy load transformers face mechanical, thermal, and electrical stresses which lead to failures of the protection systems in place. The service life of a transformer is often limited by the life time of its insulation system. Insulation failures most often develop from thermal faults, hotspots, electrical faults, or partial discharges. A failing transformer can lead to cascading failures in the power grid resulting in blackouts or brownouts for consumers. The cost of recovering from these failures can be millions of dollars, placing a great strain on the industry and the affected locales. Detecting hotspots and partial discharges to predict transformer life times is imperative and much research is focused towards these topics [8].

Transformers also develop hotspots internally when they are loaded beyond capacity or as small parts fail internally allowing heat to concentrate and buildup. At high temperatures the transformer insulating oil under goes accelerated aging which can lead to partial discharges. The Motzinger equation, which models the thermal aging process, states that the aging rate of the transformer doubles with every 6°C rise in temperature when above a maximum temperature of 98°C at the hotspot location [1]. There are thermal models based on the Motzinger equation that are able to predict the life time of a transformer based on hotspot temperatures. The IEEE has put forward several of these models for use [2][10].

The protection systems in place inside the transformer, such as the insulating oil and paper insulation on the windings go through immense stress. The aging effect caused by these electrical and thermal events leads to the degradation of the multiple electrical insulating systems. An arcing between coils, partial discharge, or electrical fault is likely to happen as the insulation degrades. These faults then damage the insulation further, accelerating the aging

process while also serving as an indicator of a failing transformer. The transformers life cycle can be measured and predicted by recording and analyzing the amount and severity of these partial discharges. Detecting these failures is of utmost importance to power providers [8].

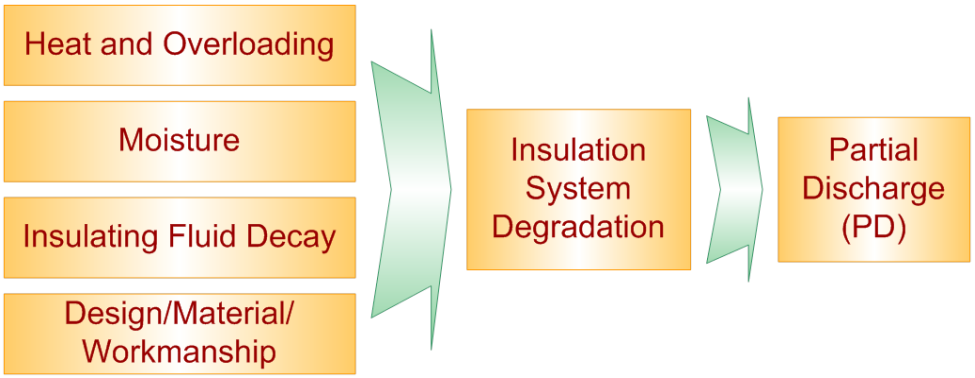

Figure 1-1
Illustration of transformer failure leading to partial discharge. Electric Power Research Institute, "Novel Sensor for Transformer Diagnosis: 2013 Research Results," Product ID: 3002000761, 2013, Used under fair use, 2014.

To determine a transformers place in its life cycle, the models developed have been coupled with new diagnostic methods based on partial discharges and hotspots. A common diagnosis tool is dissolved gas analysis (DGA) which detects the minute levels of gas generated inside a transformer during arcing and hotspot events. DGA allows for the sampling and testing of insulating oil without taking the system offline during measurement. DGA is performed by removing insulating oil from the transformer and sending it to a lab for analysis. The process typically takes several days to complete and is costly due to the procedure and high level of labor necessary. Also, with traditional DGA methods it is possible that some important but short lived gasses will diffuse from the oil before a sample can be taken or that a rapid gas buildup and transformer failure occurs before a DGA sample was possible [8].

It is also possible to detect partial discharges by listening for the acoustic signal generated during the release of large amounts of energy inherent in arcing. The sudden heating and creation of gasses from a partial discharge generates ultrasonic pressure waves in the oil. These waves travel through the oil and can be detected by an acoustic sensor placed on the transformer. However, due to the large currents there is very strong electromagnetic interference in the transformer which makes typical acoustic sensors difficult to use. A deflection or pressure sensor, such as a piezoelectric, can be used but they suffer from high signal attenuation when detecting an acoustic

wave due to being placed outside the transformer and having an oil to metal interface to pass through [3][8].

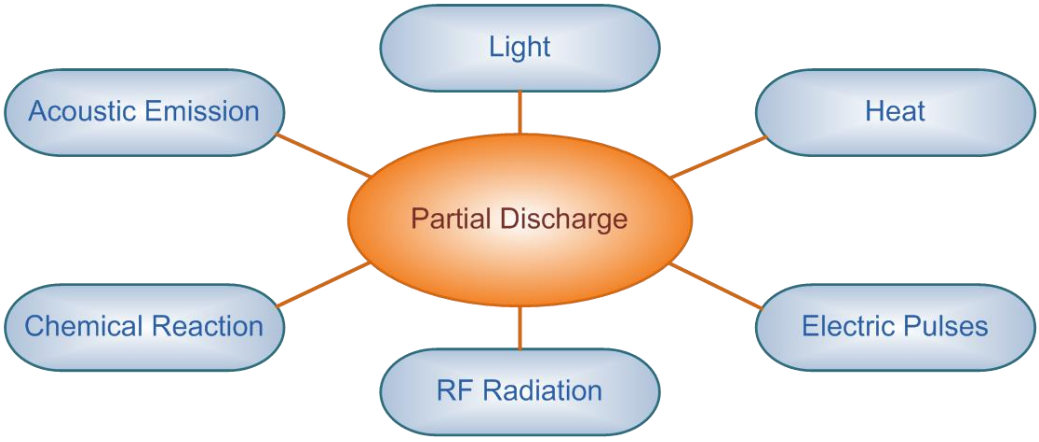

Figure 1-2
Methods for detecting partial discharges.
Electric Power Research Institute, "Novel Sensor for Transformer Diagnosis: 2013 Research Results," Product ID: 3002000761, 2013, Used under fair use, 2014.

A great, and untapped, sensor resource for transformer monitoring is fiber optic sensors. The methodology and practice of developing and deploying sensors designed for measuring pressure waves and gasses is well established. Optical fiber sensors are able to be placed in many extreme environments due to their small size and light weight while creating an almost nonexistent footprint on the system to be measured all while maintaining high sensitivity. A fiber sensor has great potential inside of a transformer due to its natural immunity to any electromagnetic interference. This type of sensor would also have the advantage of not compromising the insulation of the coils when place inside the transformer [10].

Optical fiber sensors can monitor thermal signals and dissolved gasses in real time without affecting the operation of the system. Oil can be sampled continuously, generating constant DGA data on the types and concentrations of gasses present without ever sending the oil out for analysis. Acoustic partial discharge detection is enhanced because the fiber can be placed within the system much closer to any possible signal sources. Finally, optical fibers easily handle multiplexed sensors. Distributed fault detection is possible, allowing for the mapping of hotspots or partial discharges to specific locations on the transformer using a single fiber sensor which can further reduce system cost and complexity [8].

1.2 Project Objectives

The team has already proven the viability of novel techniques for dissolved gas detection using an optical fiber as a sensing medium. We have shown detectability of hydrogen and acetylene gasses. The goal of this research step was to improve the sensitivity of our acetylene detection by improving upon the current signal to noise ratio as well as showing the sensor's non-sensitivity to other gasses that might be found in oil. Also, this research sought to improve the hydrogen sensitivity by moving to a new wavelength with stronger absorption. Finally, we sought to create a field testable prototype, consisting of a container to house the oil to be sampled as well as the aforementioned developed sensors.

2 Acetylene Sensor

2.1 Background of Acetylene Sensor

Acetylene is an important gas in DGA. Because acetylene production requires high energy, when the concentration of acetylene exceeds the limit of 5ppm it indicates arcing or severe overheating inside the transformer. The detectable limit for acetylene is low due to its strong absorption peaks with ppb levels possible in some cases. Most methods of DGA acetylene detection follow four main approaches calorimetric, chromatographic, direct absorption intensity measurement and photoacoustic detection [8].

Current DGA methods focus on extracting the dissolved gases out of the oil and measuring the concentration while in a gaseous state. This method while proven effective requires investment in removing the gas from the oil to its gaseous state and does not allow real time information gathering. The team developed a new method, based on the thermal lens effect, which determines the concentration of dissolved acetylene by directly measuring the transmission spectrum of the transformer oil. We have only shown that detecting acetylene is possible through this method currently. It is important that the dissolved acetylene modifies the transmission spectrum in a unique way to isolate it from any other dissolved gasses that may be present. The team's method is advantageous over others in that an optical fiber sensor is immune to any EMI found inside the transformer and is safe to operate while immersed in the insulating oil. The optical fiber sensor has a long lifetime and provides live DGA measurements [8]. The summation of these attributes is that this sensor provides accurate and timely DGA reports for transformer health monitoring while requiring very little maintenance for the sensor itself.

2.2 Thermal Lens Effect

When a light beam passes through a material, the sampled oil in this case, some of the energy is absorbed by that material. The absorbed energy is converted into heat, which changes the temperature of the material local to the light beam. The localized heating effects create a temperature gradient which is related to the intensity distribution of the light beam. Because the refractive index of oil is a function of temperature, a thermal lens is generated along the path of light which varies the power distribution of the beam [9]. This thermal lens power distribution varies with the absorption of the material. An absorption spectrum of the sampled oil is

generated by scanning the light source wavelength and measuring the signal retrieved [4]. The thermal lens effect is useful for the absorption spectroscopy of liquids due to its high sensitivity [5][6].

The thermal lens effect experimental setup is illustrated here. The schematic of the detection system is shown in Figure 2-1. A tunable diode laser (Newport 6328) worked as the scanning pump laser. In order to cover the entire absorption peak of 1535nm with sufficient margin, the laser was scanned from 1515nm to 1570nm. The laser output was modulated into sinusoidal shape at 100Hz by an optical modulator and the modulation signal was also sent to an oscilloscope as the trigger reference. Because the output power of the tunable laser varied with differing wavelengths by more than 30%, a 99:1 coupler was added to tap 1% power, which worked as a power reference for normalization purposes. Then the laser was delivered into the cylindrical cell by a collimator. A distributed feedback laser with wavelength centered at 1573nm worked as the probe laser and it entered the oil cell from the other end. The two collimators were aligned such that the probe laser was coupled back into fiber through Collimator A. An optical filter at 1573nm with 1nm bandwidth was placed at the output port of Circulator A to block possible reflected pump laser power. Photo detectors and transimpedance amplifiers converted optical power to electric signals, which were captured and processed by a digital oscilloscope [9].

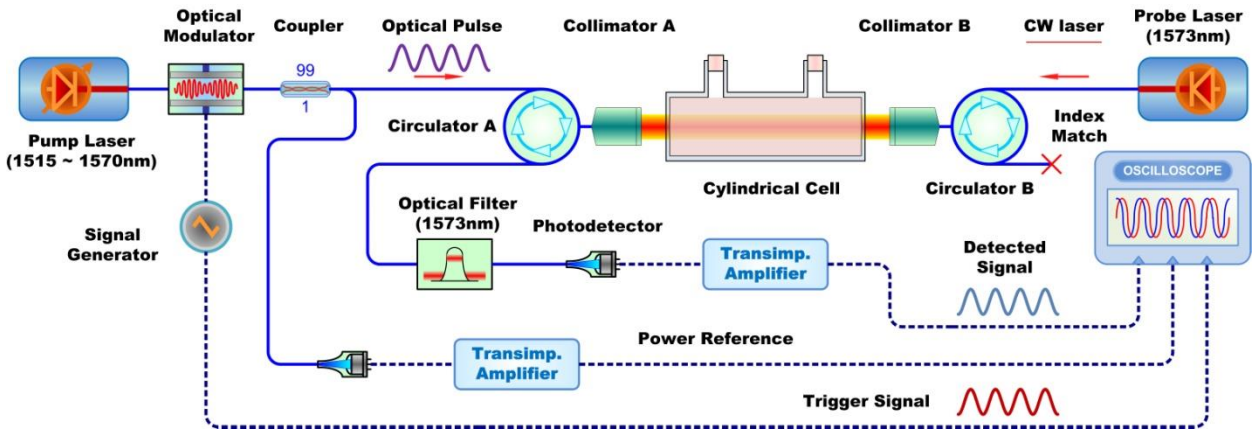

Figure 2-1
Thermal lens effect experiment schematic.
Electric Power Research Institute, "Novel Sensor for Transformer Diagnosis," Product ID: 1024193, 2012, Used under fair use, 2014.

2.3 Acetylene Probe Design

The probe design was based off of previous proof of concept work by the team. The design goal of the probe was to contain the sensors developed as well as the sampled oil in a closed system with ports for taking measurements. The probe prototype design can be broken up into three major pieces: internals, housing, and fiber interface. The internal system was designed to house wrapped fiber for hydrogen detection and also to hold a sensor probe for acetylene detection. Figure 2-2 shows the internals and housing of the prototype.

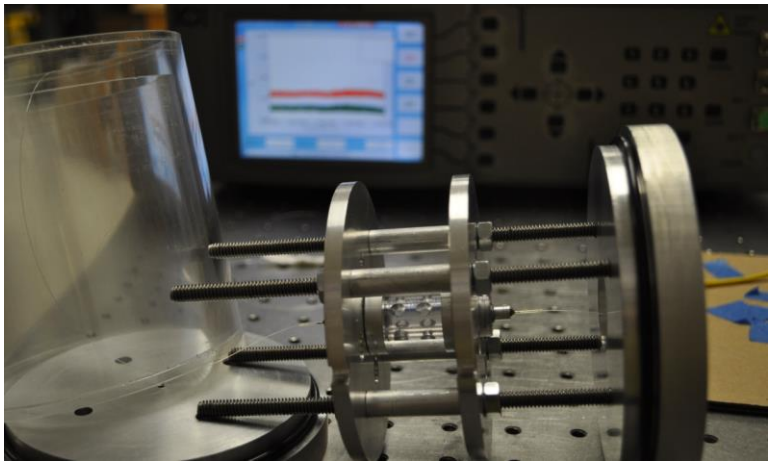

Figure 2-2
Prototype sensor showing internal skeleton and acrylic housing; Acetylene probe installed

The internal portion makes up the skeleton of the prototype for mounting the hydrogen and acetylene sensors. Four bolts attach to the base cap and provide a stand for centering the sensor mounts. Through a combination of spacers, nuts, and machined collars, two plates are attached so that they provide support for the hydrogen sensing fiber, housing shell, and a centered position for the acetylene probe.

The housing slides over the internal sensors and acts as a shell to contain the oil to be sampled. A drain is fitted to the housing to allow for oil to be cycled through the system. The housing slips over the supporting plates and fits snugly to the base cap using o-rings. To ensure a leak free fit, the four internal bolts pass through a top cap and are fitted with rubber washers and locknuts. These tighten down onto the housing, compressing the o-rings and providing a secure leak free fit around the bolts and lip of the housing. The prototype housing was initially constructed of acrylic for the purpose of displaying the internals during demonstration. The final design is made

of all aluminum which improves the reliability of the design due to decreased thermal expansion as well as being a tougher material.

Ideally, the prototype system, once constructed, remains closed and the only interaction occurs through an optical fiber connecter. The constructed prototype system remains sealed isolating the sampled oil from the outside environment while measurements are retrieved through a fiber interface. This interface is a small hole drilled through the top cap where fiber is passed outside the prototype. The hole is filled with oil resistant epoxy to prevent leaks around the fibers and provide further bracing. An outer shell is placed over the top cap and fitted for a standard APC optical fiber connector. When sealed the prototype has a connection for four optical fibers to obtain signals from the acetylene and hydrogen sensors and has two drains for oil to be cycled through the system. Figure 2-3 shows the prototype when sealed and shows the outer shell with the optical fiber interface.

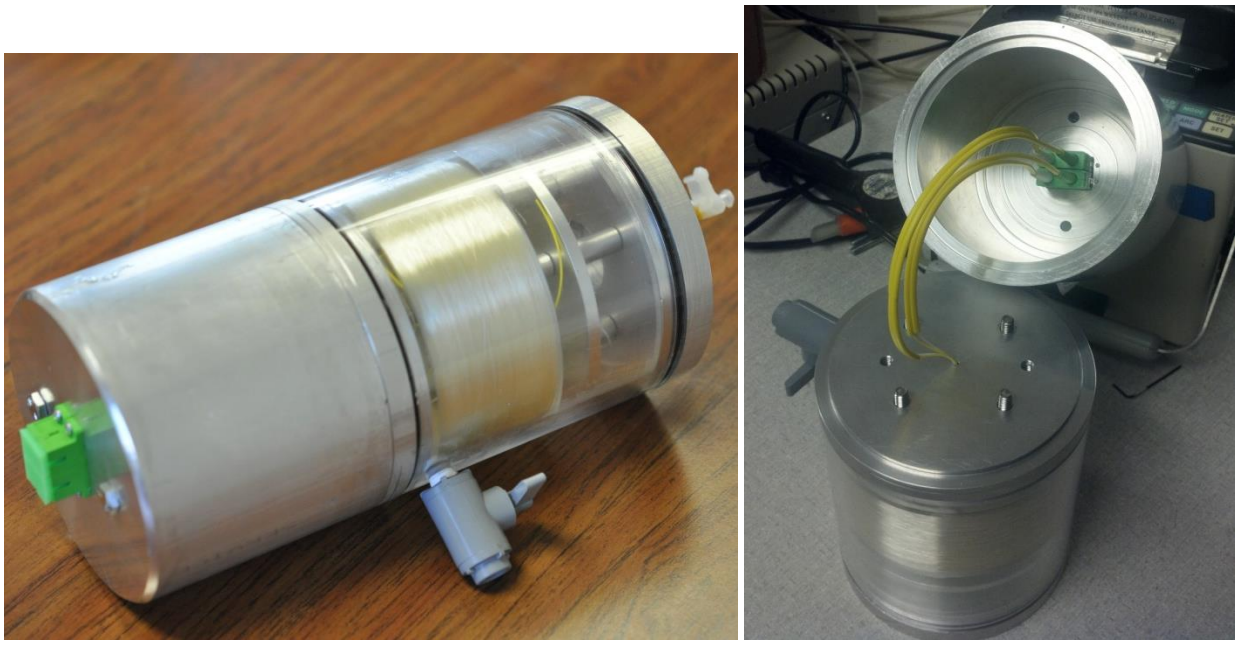

Figure 2-3
Full constructed sensor probe; Outer shell with optical fiber interface installed

The acetylene sensor is a hollow cylinder with holes around the circumference to allow for oil to flow through the probe. Optical collimators are fixed inside of swivel joints which are secured in place by screws on either end of the cylinder.

The collimator alignment is typically performed outside of the prototype system and then the entire probe is secured between two internal plates inside the prototype. Alignment is achieved by mounting the probe between two 5-axis translation stages, which are attached to the collimators, and filling the probe with oil. Light is injected into the acetylene probe and measured via CTS. Adjustments are made at each translation stage until the maximum signal level is recorded and then the swivel joints are locked into orientation by set screws.

Thus far we have been able to show that once the collimators are aligned the acetylene sensor probe can obtain a loss as low as -6.5 dB. Also, the sensor probe shows no sensitivity to thermal expansion via drifting of the signal power when held at an operating temperature of 70 °C for 24 hours. Figure 2-4 shows the demonstration sensor probe during the alignment stage. The actual probe was machined from aluminum to prevent loosening of the swivel joints caused by the thermal expansion.

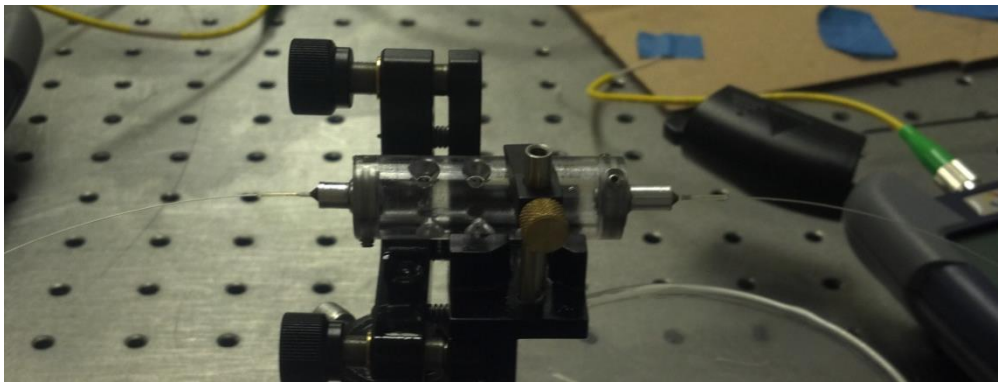

Figure 2-4
Acetylene sensor probe mounted on alignment stage

2.4 Experiment Improvement

In previous experiments we noted that a large variation in the output power of the pump laser and its low power level were limiting the detection resolution for the thermal lens method. Suggested solutions for increasing the signal to noise ratio were to use a stronger swept laser, correct the power variation of the current swept laser, or to detect the acoustic signal generated at the second harmonic of the sweeping frequency.

We approached the power variation problem by placing an electro-optical modulator (EOM) in line with the pump laser and constructing a PID controller to manage the EOM. The EOM acts as

an electronically controlled optical attenuator. The PID controller attempts to correct and level out the power variation by controlling the optical attenuation of the EOM.

To make corrections the PID requires two input values. One is the current output power from the EOM, 1% tapped power output signal, and the second is a desired value set externally. The set point value is pre-calibrated to give a desired output. The difference of the current and desired values is called the error. The PID then determines the 3 correctional terms: proportional, integral, and derivative. The proportional term is a correction based on the current error and makes up the bulk of the PID correction. Proportional correction will have a constant offset that does not reach the desired value. The integral term is a summation of previous errors and is typically the second largest contributor in PID correction. Integration will correct the offset of the proportional term but may overshoot the desired value. The derivative term is calculated by determining the change in error between corrections and usually contributes the least to correction. The derivative term corrects the overshoot of the integral term but too much contribution of the derivative will throw the system into oscillation. These three correctional terms have separate gains applied to them and are then summed into a final output correction signal that the PID supplies to the EOM. Ideally this will counter the variation of the swept laser, providing a uniform power level at each swept wavelength.

Initially, we approached the PID control method by using a microcontroller and several interfacing circuits to amplify the signal. However, this method was only moderately successful. What we discovered was that the microcontroller could not make corrections quick enough and would tend to introduce high frequency variation into the system. After the microcontroller method failed, we constructed an analog op-amp PID with much better results. However, with some further research and trials, the microcontroller method should be viable and even preferable due to the ease of adjusting the PID. A basic schematic of the analog PID controller can be found in the appendix, page A-4.

The analog PID was able to reduce the output power variation from over 30% to less than 4% variation across the swept wavelengths. Some high frequency components could not be removed via this PID method, but averaging and other techniques such as second harmonic detection reduce the effect of these components. Figure 2-5 shows the swept laser output before and after PID correction.

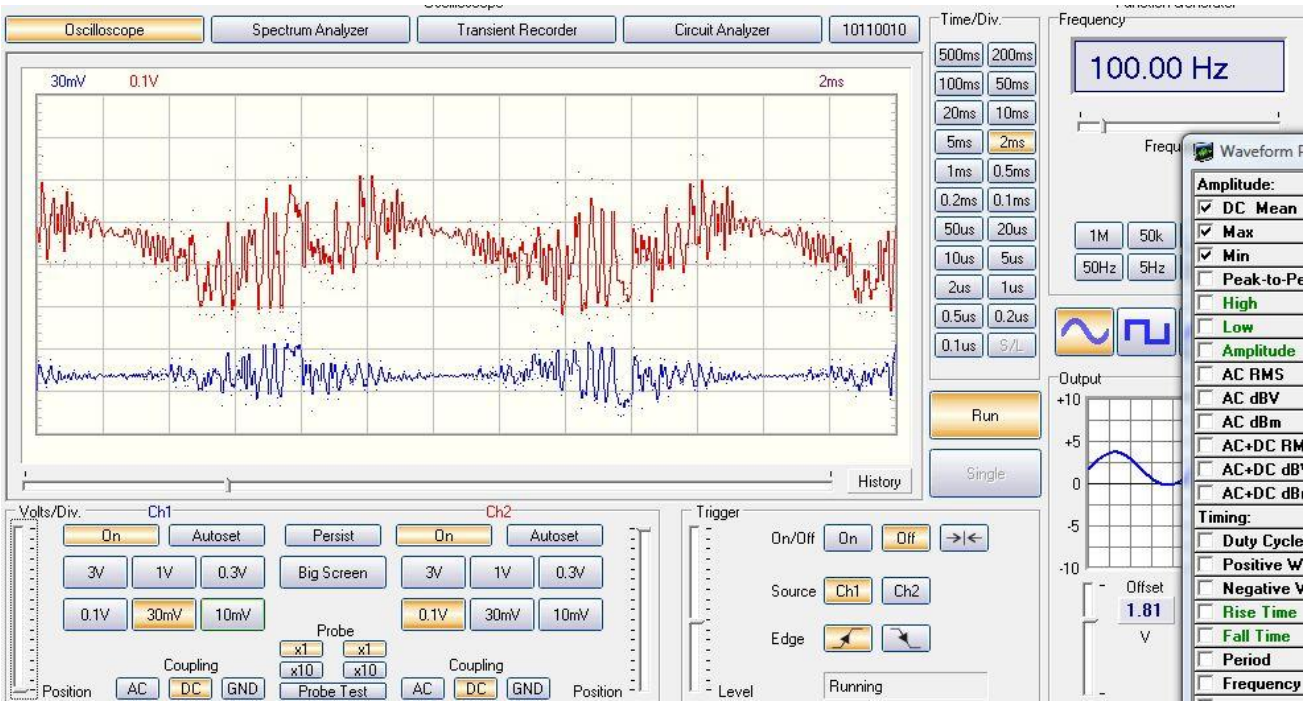

Figure 2-5
Swept laser output; Blue is output after PID correction, Red is output before PID correction

Another method investigated for increasing sensitivity was second harmonic detection. By sweeping the pump laser at 100 Hz and measuring the second harmonic, we trade for a gain in signal resolution at a loss in signal to noise ratio. The signal to noise ratio loss can be overcome with a more powerful light source. Figure 2-6 gives some illustration of the second harmonic technique. The signals are shifted along the x-axis to allow for easier viewing, each group is actually sharing the same harmonic frequency. Note that the reddish signal is the harmonics of a 0% acetylene concentration, orange and green are a 10% concentration, and blue is a 20% concentration. It can clearly be seen that for the 2nd harmonic different acetylene concentrations have signal losses proportional to their concentration, relative to the 0% baseline. Further analysis with a stronger light source, providing a higher signal to noise ratio, should lead to better quantitative results of this detection method's resolution.

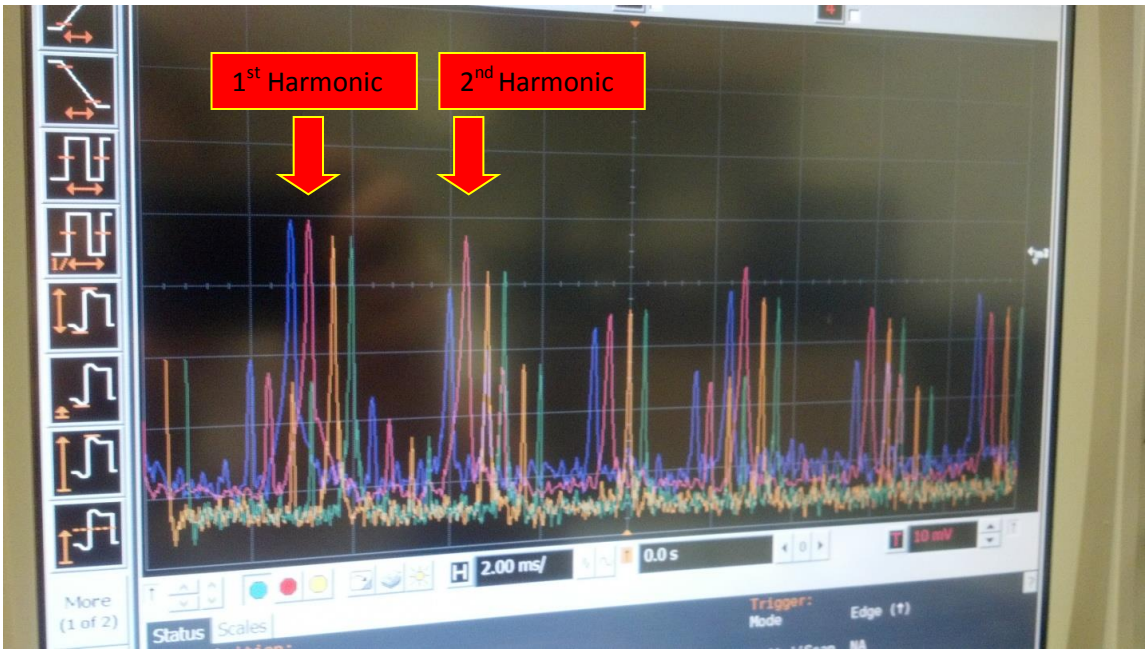

Figure 2-6
Second harmonic detection, red is 0% C_2H_2, orange and green are 10% C_2H_2, blue is 20% C_2H_2

2.5 Cross Sensitivity Experiment Setup

It is necessary to show that dissolved gasses other than acetylene do not affect absorption to prove the validity of the thermal lens effect. The team had shown previously that differing concentrations of methane do not alter absorption measurements. We sought to test two other gasses commonly found dissolved in transformer oil, carbon monoxide and hydrogen.

The system setup consisted of a 10cm spectroscopy cell to contain the oil and a Components Test System (CTS) to interrogate the sample. The CTS, acting as a light source and detector, was coupled into to the cell via two collimators and the application of degasified oil between the collimators and the cell. Alignment is maintained using a 5-axis translation stage to adjust the collimator position and angle. Orientation of the cell is recorded and preserved throughout the measuring process. Figure 2-7 shows the spectroscopy cell setup for a measurement. The CTS sweeps the light's wavelength from 1520nm – 1570nm to obtain an absorption curve of the sample. To ensure the best possible results, the curve from the CTS was averaged 20 times per sample and a further 10 samples were recorded for every measurement. Because there was potential for samples to vary during measurements as the oil settled in the cell, the measurements were repeated several times and the standard deviation between samples was recorded. The

measurement with the lowest standard deviation below a chosen threshold would then be kept for analysis [9].

The key to ensuring accurate cross sensitivity results is in the method of mixing the oil. Oil is first agitated and degasified in a vacuumed flask to maintain purity for mixing. The standard D3612-02 is followed for blending gas into a sample of Voltesso 35 insulating transformer oil. Sample oil and gas are mixed in volumes of 50 ml of oil except in the case of the cross sensitivity gas sample. Gas is extracted from the cylinder by syringe for measurement before being injected into the sample oil. Oil with acetylene concentrations of 0%, 5%, 10%, and 20% are made for analysis as a baseline comparison. For the cross sensitive gas analysis, oil is mixed in 200 ml volumes with a 5% acetylene concentration and then separated into 50 ml volumes and mixed with concentrations, relative to the acetylene, of 10%, 50%, and 100% of the cross sensitive gas. This is done to ensure that the acetylene baseline is the same for all cross sensitive samples. Once prepared the oil is injected into the spectroscopy cell for measurement.

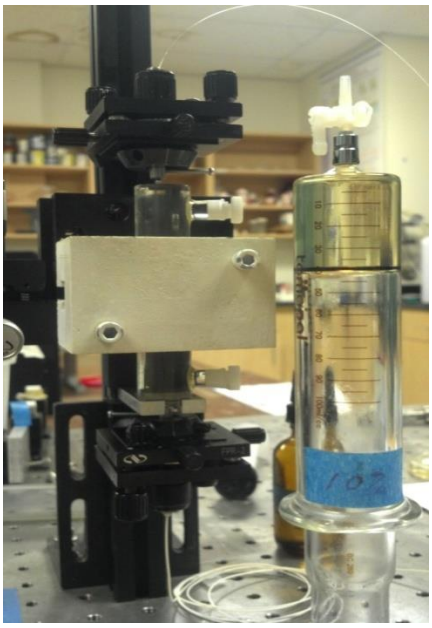

Figure 2-7
Spectroscopy cell prepared for measurement

Measurements from the CTS are recorded in Matlab where the best result is kept and multiple sample measurements can be averaged. Once measurements are taken and an absorption curve is obtained for each sample, the 0% acetylene concentration is subtracted as a baseline and all

curves are normalized for analysis. Figure 2-8 and Figure 2-9 show plots of the normalized curves from the hydrogen and carbon monoxide cross sensitivity measurements.

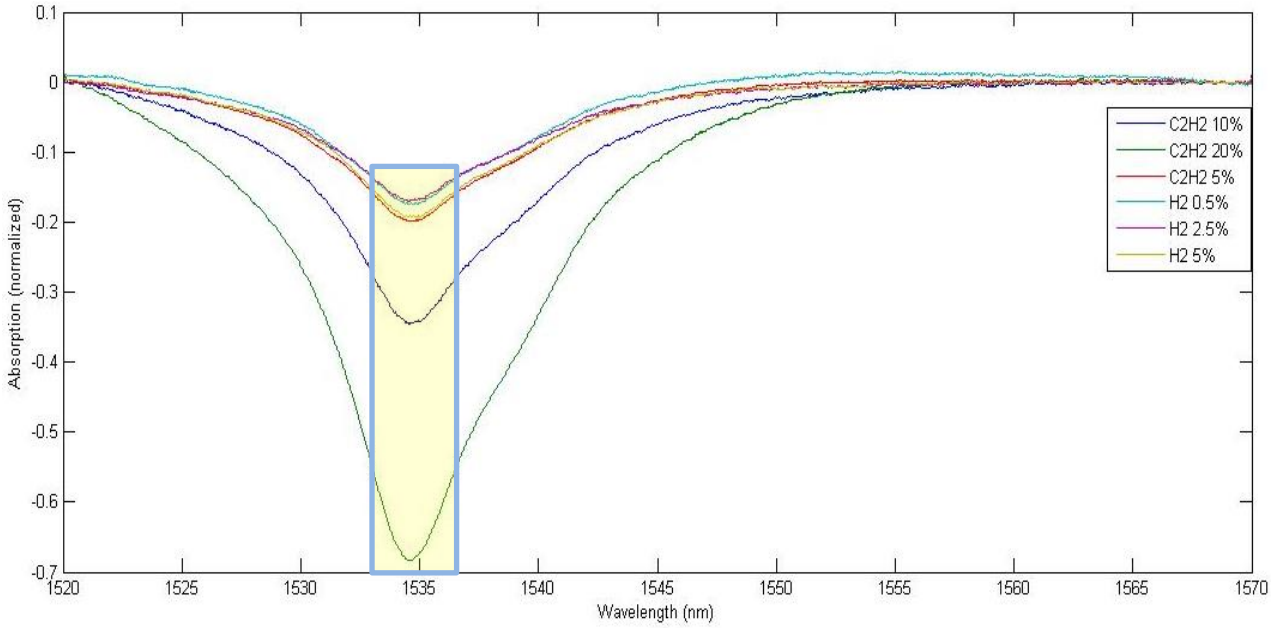

Figure 2-8
Normalized absorption plot of hydrogen cross sensitivity test with absorption region highlighted

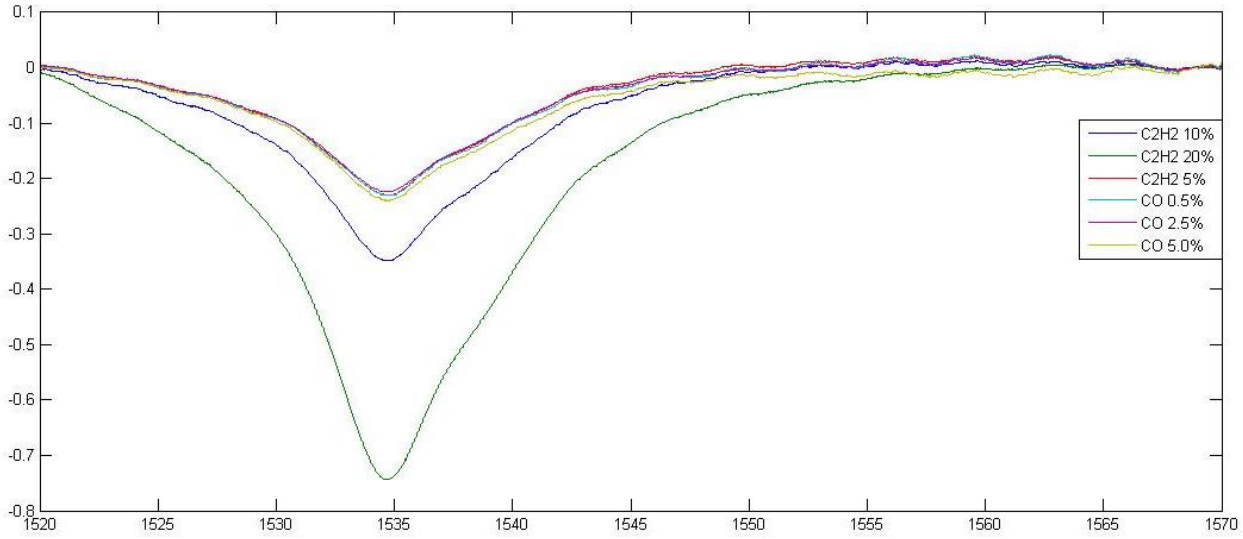

Figure 2-9
Normalized absorption plot of carbon monoxide cross sensitivity test

The highlighted region centered on 1535 nm is considered the absorption region. Cross sensitivity results are determined from the data in this selection. Note that the 0.5%, 2.5%, and 5% legends for hydrogen are respectively the 10%, 50%, and 100% relative concentrations mentioned. Further analysis confirms the non-sensitivity of the sensor to hydrogen and carbon monoxide gases.

2.6 Cross Sensitivity Results

The absorption region highlighted in Figure 2-8 falls between the wavelengths of 1533nm - 1536nm. This region was chosen for both H_2 and CO analysis. Table 2-1 shows the cross sensitivity analysis. The term slope is the ratio of that sample's absorption relative to a 20% C_2H_2 sample. STD is the standard deviation of the calculated slope for each measurement.

Conc. (Gas)	Slope	Std		Conc. (Gas)	Slope	Std
20% (C_2H_2)	1.00	0.0078		20% (C_2H_2)	1.00	0.0093
10% (C_2H_2)	0.473	0.0037		10% (C_2H_2)	0.535	0.0035
5% (C_2H_2)	0.311	0.0023		5% (C_2H_2)a	0.305	0.0029
0.5% (CO)	0.311	0.0027		0.5% (H_2)b	0.275	0.0056
2.5% (CO)	0.292	0.0033		2.5% (H_2)b	0.256	0.0038
5.0% (CO)	0.322	0.0020		5.0% (H_2)a	0.299	0.0023

Table 2-1
Carbon monoxide and hydrogen cross sensitivity analysis

The table shows a slope near 0.5 for 10% C_2H_2 which falls in line with previous measurements. Deviation is likely due to the relatively large error in measuring gas. The 5% C_2H_2 concentration has an expected slope of about 0.30 which the experimental results match. Moving to the comparison of CO and H_2 gases dissolved in oil as well, we can see that the slope remains very similar to that of the 5% C_2H_2 sample. The subscripts for the H_2 measurements denote oil samples that were mixed from same acetylene container. Samples marked with 'a' came from the same 5% C_2H_2 container, and samples marked 'b' shared a C_2H_2 container as well. This explains the difference between H_2 measurements compared to the CO measurements. All CO samples came from the same C_2H_2 container. Considering the error in measuring gases and dissolving

them into the oil, this analysis shows the detection method has no sensitivity to dissolved gases other than acetylene.

2.7 Sensor Limits of Detection

The same experimental setup to determine cross sensitivity was used to measure the system's current limit of detection as well. The relationship of relative absorption to concentration follows a linear regression as expressed below.

$$S(\lambda, C1, t) - S(\lambda, C2, t0) = m * \beta(\lambda) + \mathrm{D} \qquad (2.1)$$

where S is a logarithmic term of the absorption based on wavelength, acetylene concentration, and time, which becomes the ratio called slope; m is a constant calculated empirically from the experiment; ß(λ) is acetylene concentration; and D is dependent on oil aging, which is 0 for this case. The 20% acetylene absorption is used as a reference, in place of C2, and other absorption curves are measured as C1. Using this equation and applying it in terms of the above table, we obtain the form of:

$$slope = m * Conc. \qquad (2.2)$$

We choose the acetylene measurement with the smallest standard deviation from the table results. As an example, there exists a measurement of 5.00% acetylene with a slope of 0.311 and standard deviation of 0.002 which can be used to solve for *m =6.22*. Now taking into account the standard deviation of this measurement we can determine the reliable range of concentration as:

$$0.311 \pm 0.002 = 6.22 * Conc. \qquad (2.3)$$

$$Conc. = 5.00\% \pm 0.04\%$$

The range of ±0.04% translates into a sensor detection resolution of 800 ppm. However, for this method of measurement we are approaching the limit of the CTS's detection resolution, which was found to be very near to 0.0017, and we may likely see sensor resolution improvements from a better interrogation system.

2.8 Acetylene Conclusion

The measuring of dissolved acetylene in oil is crucial for detecting partial discharges. To ensure an accurate analysis, the measured acetylene signal should be isolated from any other possible dissolved gas signals. Thus far the sensor has shown to be non-sensitive to three other gases that

can be found dissolved in transformer oil; hydrogen, carbon monoxide, and methane. Further cross sensitivity analysis of other gasses can be performed as necessary to verify the reliability of acetylene detection. The current resolution of the sensor is tied to the detection limits of the interrogation equipment. Resolution should be improved through the use of better equipment [9].

Detection of a photothermal signal for determination of acetylene concentration in transformer oil is a novel method and it is still being developed. In previous experiments we were able to detect the photothermal signal at low resolutions. We have since made improvements in our detection capabilities by stabilizing the pump laser's output with PID control and by using correlation detection methods to capture the second harmonic of the sweeping frequency. Further improvements will come about through the use of higher quality and more powerful pumping light sources and photodetectors.

3 Hydrogen Sensor

3.1 Background of Hydrogen Sensor

Gaseous hydrogen does not typically have strong absorption in the infrared range we are operating in because there is no dipole moment. As the hydrogen diffuses into the fiber and becomes trapped in the glass, the molecules are polarized locally. This polarization occurs due to the hydrogen bonding to oxygen in the lattice structure and creating OH^- molecules. This local polarization produces infrared absorption as shown in Figure 3-1 [7]. The fundamental absorption peak located at 2.42μm is due to the hydrogen stretching vibration. The other absorption peaks shown are due to a combination of the hydrogen rotational vibration and the hydrogen stretching vibration or a combination of the hydrogen stretching vibration and the SiO_4 lattice [7][8]. There are three main absorption points apparent at 1.24μm, 1.88μm, and 2.42μm. Initial experiments were performed at 1.24μm. However, the best signal to noise ratio occurs at 1.88μm, which is where the current sensing is performed at.

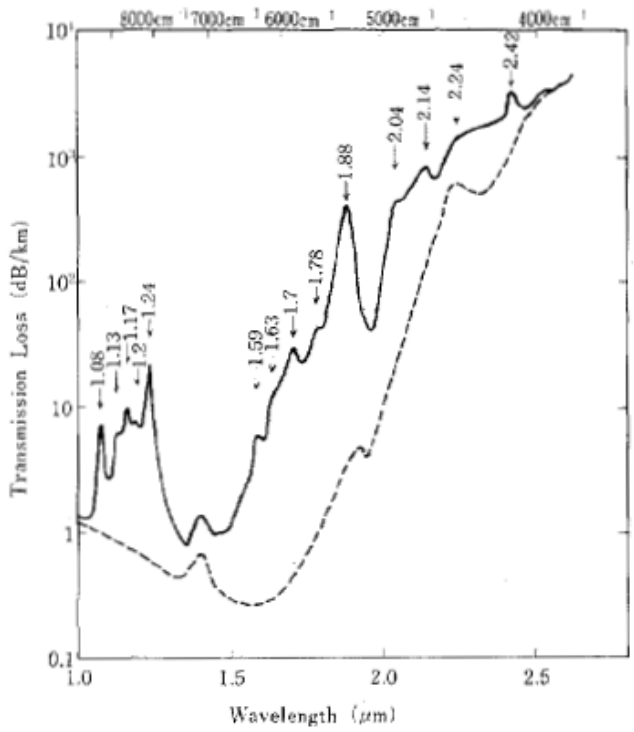

Figure 3-1
Infrared absorption of hydrogen when diffused in silica fiber.
Mochizuki, K., et al., *Behavior of hydrogen molecules adsorbed on silica in optical fibers*. Quantum Areas in Communications, IEEE Journal on, 1984. 2(6): p 842-847, Used under fair use, 2014.

The fiber losses at the most prominent peaks of the absorption curve were calculated for differing hydrogen concentrations and are shown on Table 3-1 [8][11][12]. The large peak and valleys near 1.88μm signifies an ideal detection wavelength due to the high signal to noise ratio.

Wavelength (μm)	Fiber loss w/o H_2 (dB/km)	Fiber loss increase for 1bar H_2 (dB/km)	Fiber loss variation at 50ppm H2
1.24	~0.8	~8	~0.003dB (0.1%) @10km
1.88	~2.5	150~200	~0.09dB (2%)@10km
2.42	~1800	~3500	~0.0009dB(0.02%) @10km

Table 3-1
Fiber Loss at Possible Absorption Lines for Different Hydrogen Concentration.
Dong, Bo, "Fiber Optic Sensors for On-line, Real Time Power Transformer Health Monitoring," Ph.D. dissertation, Dept. of Electrical and Computer Engineering, Virginia Polytechnic Institute and State University, Blacksburg VA, 2012, Used under fair use, 2014.

The team originally designed the hydrogen sensor to be operated with light at the 1240nm wavelength and consisted of 850 meters of optical fiber wound onto a mandrel and inserted into the probe. The design was updated to 200 meters of optical fiber using light of wavelength 1880nm. The optical fiber mandrel has holes drilled to allow for oil to flow and contact all of the sensing fiber. Hydrogen detection is based on the phenomenon of hydrogen diffusion into silica optical fibers, wherein any other hydrocarbon molecules present in the oil are too large to penetrate into the silica fiber. The diffusion of hydrogen into fiber increases the optical loss that the team can then measure and use to determine the amount of hydrogen present in oil. It was found that the response time of the sensor correlates to the diameter of the fiber. Hydrogen must diffuse through the fiber material towards the core. A smaller cladding wall means hydrogen reaches the core sooner. To improve response time, the team decided to chemically etch the fiber cladding near to the core. Figure 3-2 shows the hydrogen sensing fiber wrapped and positioned inside the prototype, the acrylic outer housing is used for illustration purpose [10].

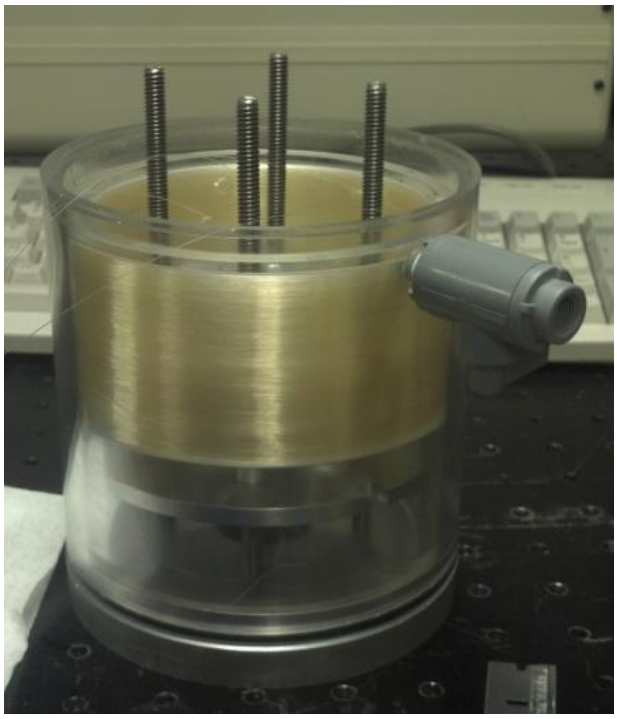

Figure 3-2
Hydrogen sensing fiber wound and inserted into prototype

3.2 Sensing Fiber Fabrication

An optical fiber with a cladding diameter just thick enough to cover the core is ideal, but the manufacture of such a fiber is costly. Chemical etching was chosen as a reliable and cost-effective approach to obtaining custom sized fiber from off the shelf supplies. The dual-acrylate coating is removed by a strong acid and the glass cladding is etched away by the use of hydrofluoric acid. The team decided to make a new mandrel out of Teflon because acrylic cannot withstand the extreme conditions present when etching.

The dual-acrylate found on fiber is a protective coating consisting of a hard outer layer and a soft inner layer. This coating is removed chemically by the use of 3-parts sulfuric acid to 1-part hydrogen peroxide, also known as piranha solution. The solution heats rapidly and reacts vigorously with organic matter. Due to the relatively high coefficient of thermal expansion of Teflon, the team allowed the piranha to cool slightly so as not to put unnecessary stress on the fiber during the decoating process. The entire decoating process takes 6-8 hours while keeping the acid at a stable temperature of 50 °C. The mandrel with wrapped fiber is removed from the

acid and placed in a water bath to clean away any residual acid. It is then air dried before continuing.

The fiber cladding diameter is reduced by hydrofluoric acid etching. Hydrofluoric acid does not react with plastic but is uniquely able to eat away glass. At this stage the fiber is very fragile without its coating. Reducing the cladding diameter relieves some of the intrinsic stress on the wrapped fiber but makes it more susceptible to impact. Therefore, the team machined a holding container to protect the fiber and ensure acid coverage. The etching rate of hydrofluoric acid is about 1um per minute submerged. Etching rates vary based on the freshness of the acid so the optical loss was also monitored during the etching so as not to exceed -3 dB signal attenuation. A cladding diameter of 80um was desired for a multimode fiber with a 50um core. The reason for multimode fiber being used is due to the lack of commercial light sources operating at the desired wavelength capable of being coupled to single mode fiber. Verification of the fiber cladding diameter was done via micrometer and microscope. A water and air bath takes place again to clean the fiber after the etching step.

The fiber is now extremely fragile at this stage. Epoxy is placed where the fiber passes through the mandrel in order to isolate the etched fiber from any strain placed on the unetched fiber during system assembly. A thin sheet of paper is wrapped around the mandrel when the fiber is ready to be placed inside the probe. The paper protects the fiber from any external stresses that might happen during assembly and also prevents the fiber from touching any part of the metal probe housing. Once inserted in the system, fiber connectors are spliced to the sensing fiber and passed outside the probe housing to provide measurement access. The system can then be completely sealed and filled with oil. Figure 3-3 shows the Teflon mandrel before etching and after insertion. Figure 3-4 shows the completed system assembled and prepared for sealing and oil insertion.

Figure 3-3
(a) Teflon mandrel wrapped with 200 meters fiber before etching.
(b) Mandrel inserted into probe housing after etching

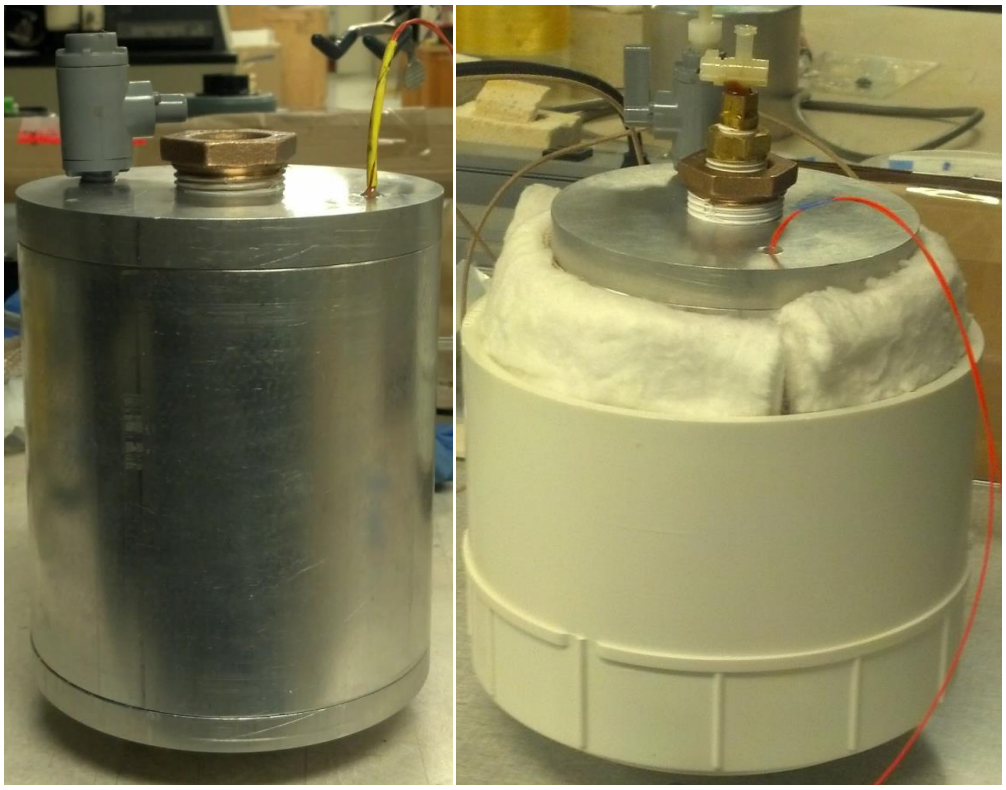

Figure 3-4
(a) Sensor probe assembled and ready for oil insertion and measurement
(b) Sensor probe filled with oil and measurement taking place

3.3 Hydrogen Oil Preparation

The team produced their own oil containing dissolved hydrogen for the purpose of testing and calibration. To remove any existing atmospheric gas contamination from the oil, it was placed in an airtight container where a vacuum would be pulled and the oil could be agitated by a magnetic stirrer. This setup was able to degasify the oil in a few hours. The oil used was Voltesso 35 and it was injected with ultra-high purity hydrogen gas. A measured amount of oil was taken by syringe for the hydrogen injection. Hydrogen was mixed into the oil by volume using a separate gas filled syringe. The syringe system was pressurized and agitated to accelerate the gas dissolving process. For example, a 5% hydrogen concentration was achieved by injecting 100mL of oil with 5mL of hydrogen gas. Smaller concentrations, such as 0.5%, can easily be achieved by diluting already hydrogenated oil with pure degasified oil. Initial measurements were made with a high gas concentration of 5%.

3.4 Light Source Coupling

The team had initially planned to use single mode fiber as the sensing fiber due to its low cost and small core diameter which allowed for a faster possible response time. It was discovered that there are very few products on the market for broadband or tunable light sources near the 1.88µm range. So, the team attempted to develop a light source by coupling light from an LED source centered at 1.90µm into single mode fiber. The LED was chosen such that its center wavelength was slightly tunable via TEC and the output light was concentrated by a parabolic reflector. Figure 3-5 describes the spectra and far field pattern of the selected LED.

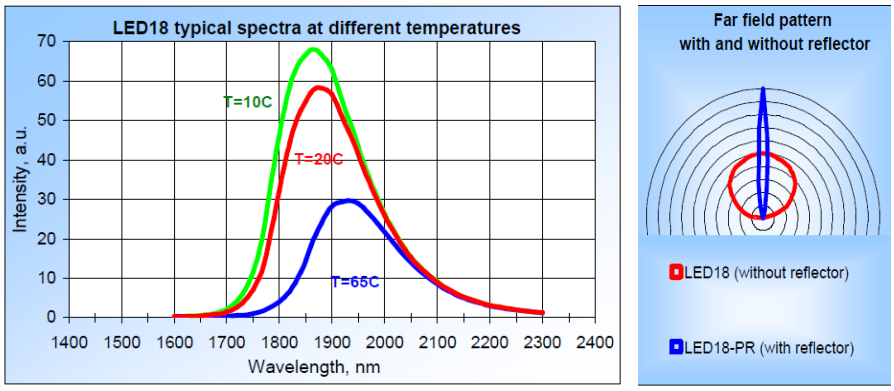

Figure 3-5
(a) LED spectral density based on operating temperature
(b) LED far field pattern

Direct coupling, lens coupling, and lens coupling with a fiber collimator were approached as solutions to guiding light into single mode fiber and multimode fiber. Direct coupling was performed by placing the optical fiber very near to the active area of the LED. However, the large active area relative to the fiber core size prevents any meaningful amount of light from entering the fiber. The lens method was slightly better but still suffered from inefficiencies due to the active area size and non-divergence of the light. Figure 3-6 illustrates two coupling methods.

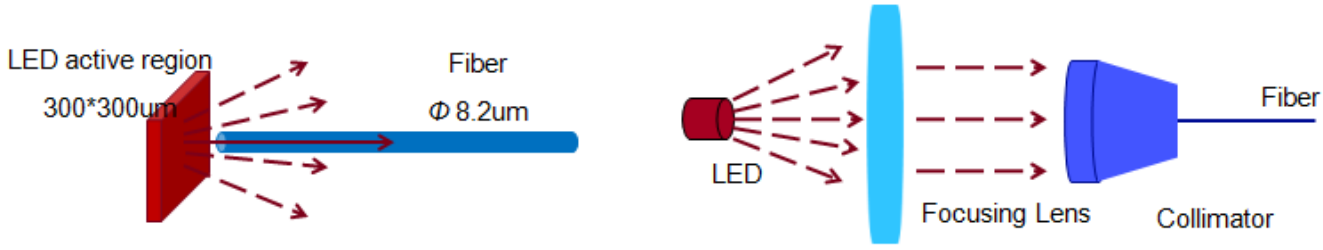

Figure 3-6
(a) Direct coupling of LED
(b) Lens and collimator coupling

The results of these coupling trials are displayed in Table 3-2. The fibers used were multimode fiber with a 50um core diameter, and singlemode fiber with an 8.2um core. The LED power was 0.9mW. Very little light was able to be coupled into the fiber during any of the trials. The team eventually decided to use a halogen lamp as a broadband lamp source coupled to multimode fiber. The lamp was able to provide a substantial enough amount of light to take measurements.

	Direct Coupling	Lens Coupling	Collimator Coupling	Lens + Collimator
Multimode Fiber	292nW	652nW	24nW	40nW
Singlemode Fiber	3nW	NA	2nW	NA

Table 3-2
LED to fiber coupling results

3.5 Hydrogen Sensor Results

The system configuration is displayed in Figure 3-7 with key components highlighted. The measurement process proceeds as follows: Highlighted in orange is a broadband light source coupled to multi-mode fiber. The light passes into the sensor probe, highlighted in red, through a small hole in the end cap. The hydrogen sensitive fiber is inside the probe along with the Voltesso 35 oil to be sampled. The object highlighted in green is a heating system built by the

team to bring the oil and probe to a controlled temperature, simulating the expected operating temperature of a transformer. The fiber passes out of the system to an optical spectrum analyzer, highlighted in blue. The computer, highlighted in yellow, is used to capture, analyze, and display the data from the spectrum analyzer.

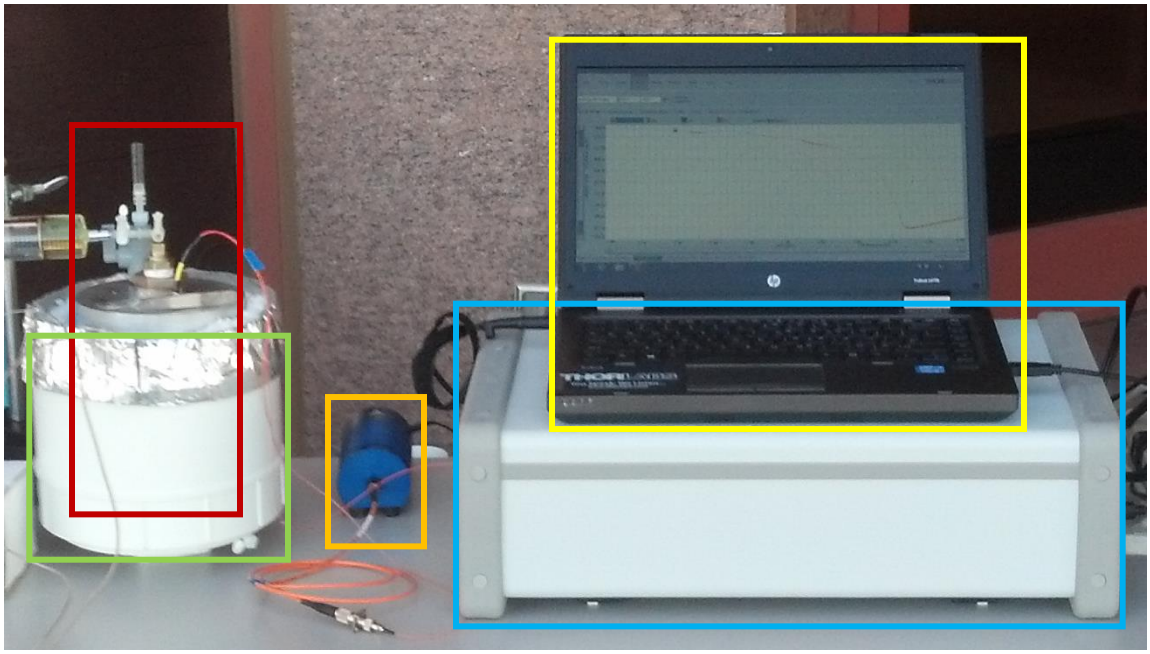

Figure 3-7
Testing configuration displaying sensor probe (red), heating pot (green), broadband light source(orange), OSA (blue), and computer for signal display (yellow)

Since there was no strong light source centered at 1.88um available in the market, the team decided to use a broadband light source, HL2000 from OceanOptics. The halogen light source was coupled to the multimode fiber used in the hydrogen sensor probe. The power density of the halogen light source was about -55dBm. The lead-in fiber cable of the probe connects to the lamp while the lead-out fiber connects to an optical spectrum analyzer (Thorlabs OSA203), which measures the power density along multiple wavelengths. The detection range of the OSA covered both 1.24um and 1.88um absorption wavelength. Two absorption dips show on the spectrum simultaneously as hydrogen diffuses into the silica fiber. To reduce the response time of the sensor, heating tape and insulation were used to increase the probe temperature.

Before connecting the probe to the OSA, a simple experiment was conducted to compare the absorptions at 1.24um and 1.88um. One meter of multimode fiber, previously kept in a high

pressure environment of Hydrogen, was connected to the light source and the OSA. Figure 3-8 is the transmission spectrum acquired from the OSA. A small dip at 1.24um and a much deeper dip at 1.88um can be observed from the red curve, indicating the latter absorption is at least 10 times greater than the former one. There are also series of very sharp spikes near 1.4um and 1.9um in both curves, which come from the intrinsic absorption of the halogen gas in the bulb. These spikes can be filtered out easily and don't affect the measurement at 1.88um.

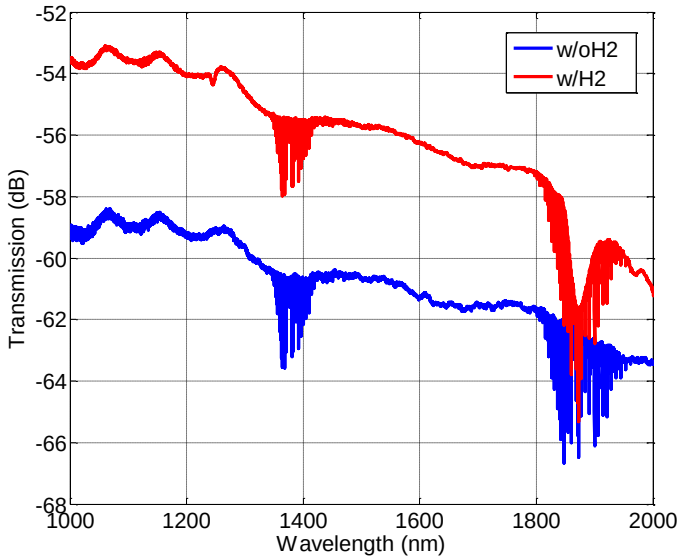

Figure 3-8
Transmission of MMF with and without Hydrogen diffusion

The first probe was made with 100m multimode fiber inside for demonstration. Since the absorption depth is proportional to the fiber length, another probe with 200m fiber was made to increase the sensing response. The first test was measuring the response to 5% hydrogen dissolved in oil. The probe was filled with about 650ml transformer oil and heated to 40C with the spectrum data taken every 40min. Figure 3-9(a) is the spectrum change over time and Figure 3-9(b) is the normalized absorption. The normalization process eliminated the offset induced by power fluctuation, filtered out the intrinsic halogen absorption spikes and normalized the base line for absorption.

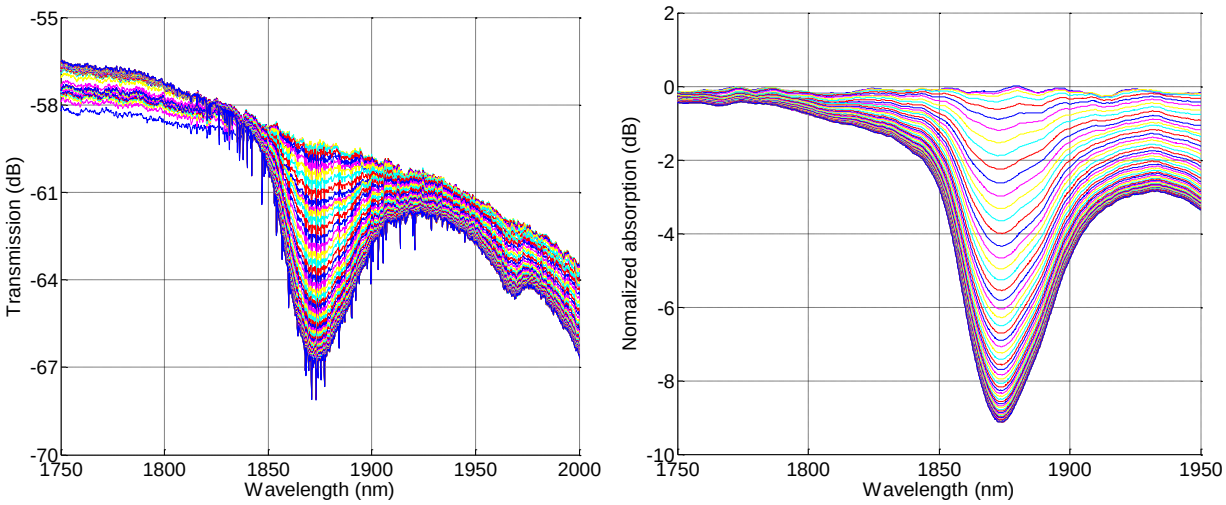

Figure 3-9
(a) Transmission change over time (b) Normalized absorption at 1.88um

To extract the absorption depth, Gaussian curve fitting was applied to Figure 3-9(b) as well as the similar absorption at 1.24um. The result is shown in Figure 3-10. The maximum absorption for 1.88um and 1.24um are about 9dB and 0.6dB respectively at 5% hydrogen concentration. The 80% response time is about 16 hours. Further measurements were made using oil with 0.5% hydrogen concentration. The measured signal absorption was about 0.9dB, which falls in line with predictions based on the 5% measurement. There were two issues found in this experiment: long response time and inaccurate demodulation scheme. Ideally, the response time should be less than a couple of hours and further increase of the temperature should improve the sensor response time. For the demodulation process, as shown in Figure 3-9(b), the absorption dip is not symmetrical, which implies that Gaussian curve fitting may not be the best candidate for data extraction. The area below the base line can also be calculated as the absorption measurement.

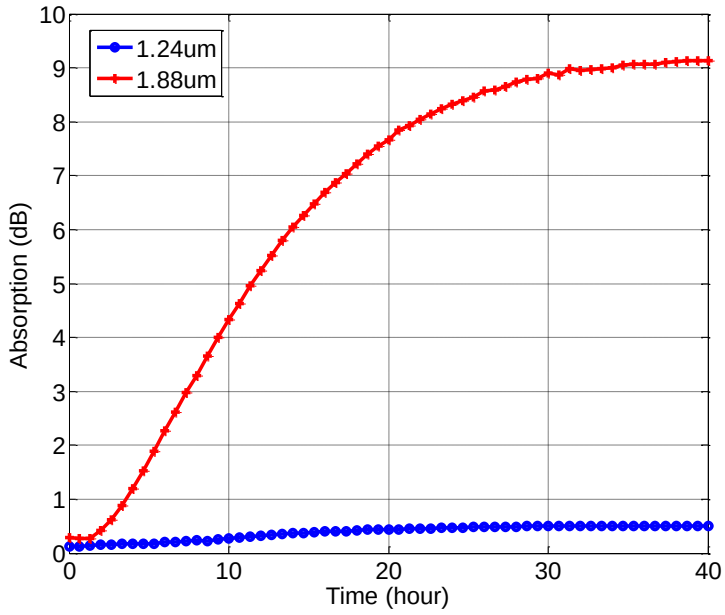

Figure 3-10
Absorption depths at two wavelengths for 5% hydrogen concentration

The diffusion of hydrogen from oil to fiber and from fiber back into oil is a constant process as the system seeks equilibrium. After a measurement is complete it is desirable to remove the existing hydrogen from the system in preparation of another sample. Removal of the oil from the system allows for hydrogen to diffuse out of the fiber. The rate at which equilibrium is reached with the atmosphere can be expedited by heating the system. The team has found that elevating the probe temperature to 50°C during this process can evacuate hydrogen from the fiber in 10-12 hours for 5% hydrogen concentrations. The equilibrium time is correlated to the starting hydrogen concentration and probe temperature. Therefore, it can be expected that smaller hydrogen concentrations will evacuate from the fiber faster.

3.6 Hydrogen Conclusion

Redesign of the sensor probe has allowed for improvement in hydrogen detection capabilities. By switching light sources the research was able to obtain a near ten-fold signal improvement over previous work. The sensor probe constructed is a field testable design and was used at the Pheonix Taskforce to record and present results in real time.

Further signal improvements can be expected from the use of a stronger light source or a source suited for single mode fiber. The response time of the sensor will decrease as the diameter of the

sensing fiber decreases. Increasing the length of the sensing fiber wrapped on the mandrel will improve the minimum detectable limit for hydrogen. Moving forward, the research would be best served by locating an acceptable light source for singlemode fiber centered at the operating wavelength.

4 Summary

Across the life span of this project the team sought to improve upon previous milestones by increasing the sensitivity of both acetylene and hydrogen sensors while designing and producing a field testable prototype. While there were difficulties to overcome, we were able to produce measurable forms of success in all regards.

We have made improvements in our acetylene detection capabilities by stabilizing the pump laser's output with PID control and by using correlation detection methods to capture the second harmonic of the sweeping frequency. Also, to ensure the reliability of the acetylene detection method, cross sensitivity testing was performed on two gasses also found in transformer oil. Thus far, we have shown that our acetylene sensor has no sensitivity to hydrogen, carbon monoxide, and methane. More gases can be analyzed quickly and easily in the future. The current resolution of the acetylene sensor is tied to the detection limits of the interrogation equipment. Moving forward further progress should come about from the use of higher quality light sources and detectors.

The hydrogen sensor saw a large increase in sensitivity at the 1880nm absorption peak compared to 1240nm peak from previous designs. There was great difficulty in finding a suitable light source and fiber for operation at 1880nm. Time was taken to fabricate our own custom sensor. This particular sensor will benefit greatly with the use of a powerful commercial light source coupled into a singlemode fiber.

Finally, we produced a functioning prototype containing the hydrogen sensor and took it to an EPRI sponsored conference to present the work and proof of operation.

Reference

(1) G, Betta and A. Pietrosanto, “An Enhanced Fiber-Optic Temperature Sensor System for Power Transformer Monitoring”, IEEE Trans. Instr. Meas.

(2) “IEEE guide for loading mineral-oil-immersed power transformer rated in excess of 100 MVA (65°C),” IEEE/ANSI C.57.115.1991

(3) R. Meunier, G. H. Vaillancourt, “Propagation behaviour of acoustic partial discharge signals in oil-filled transformers,” 12th International Conference on Conduction and Breakdown in Dielectric Liquids, Roma, Italy,1996

(4) Gordon, J. P., Leite, R. C. C., Moore, R. S., Porto, S. P. S. and Whinnery, J. R. (1965). "Long-Transient Effects in Lasers with Inserted Liquid Samples." Journal of Applied Physics **36**(1): 3-8.

(5) Gupta, M. (1980). "Thermal diffusivity measurements using a pulsed dual beam thermal lens technique." Appl. Phys. Lett. **37**(6): 505.

(6) Long, M. E., Swofford, R. L. and Albrecht, A. C. (1976). "Thermal lens technique: A new method of absorption spectroscopy." Science **191**(Copyright 1976, IEE): 183-185.

(7) Mochizuki, K., et al., *Behavior of hydrogen molecules adsorbed on silica in optical fibers*. Quantum Areas in Communications, IEEE Journal on, 1984. **2**(6): p 842-847

(8) Dong, Bo, “Fiber Optic Sensors for On-line, Real Time Power Transformer Health Monitoring,” Ph.D. dissertation, Dept. of Electrical and Computer Engineering, Virginia Polytechnic Institute and State University, Blacksburg VA, 2012

(9) Electric Power Research Institute, “Novel Sensor for Transformer Diagnosis,” Product ID: 1024193, 2012

(10) Electric Power Research Institute, “Novel Sensor for Transformer Diagnosis: 2013 Research Results,” Product ID: 3002000761, 2013

(11) Mochizuki, K., et al., *Influence of Hydrogen on Optical Fiber Loss in Submarine Cables.* Selected Areas in Communications, IEEE Journal on, 1984. **2**(6): p. 842-847.

(12) Beales, K.J., D.M. Cooper, and J.D. Rush, *Increased attenuation in optical fibres caused by diffusion of molecular hydrogen at room temperature.* Electronics Letters, 1983. **19**(22): p. 917-919.

Appendix

Prototype model and drawings

Sensor prototype displaying acetylene sensor probe centered between plates

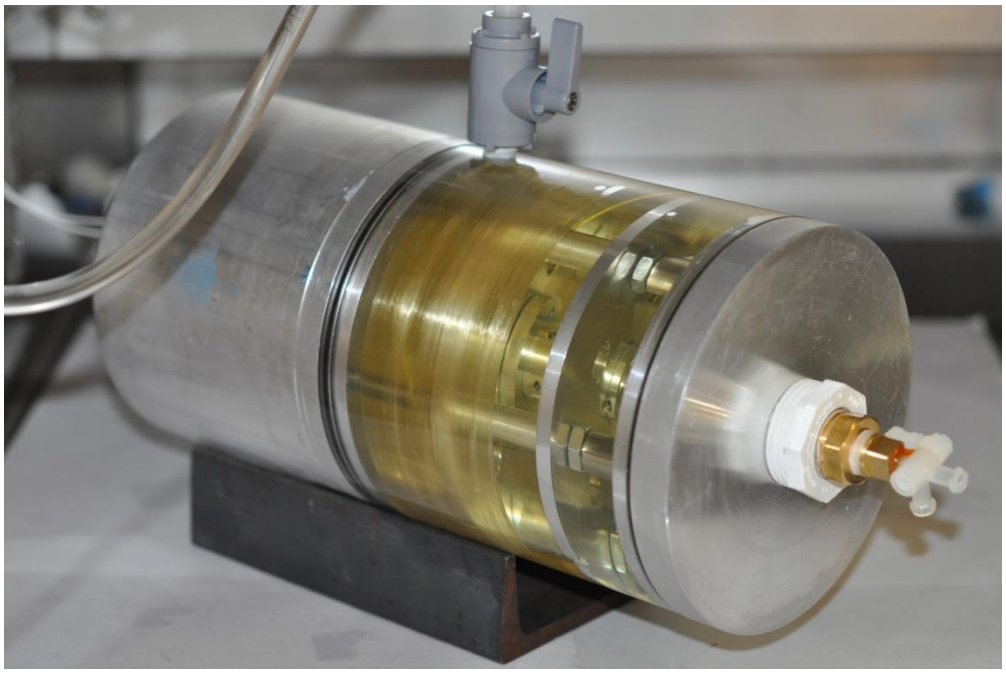

Sensor prototype filled with oil during hydrogen sensing testing

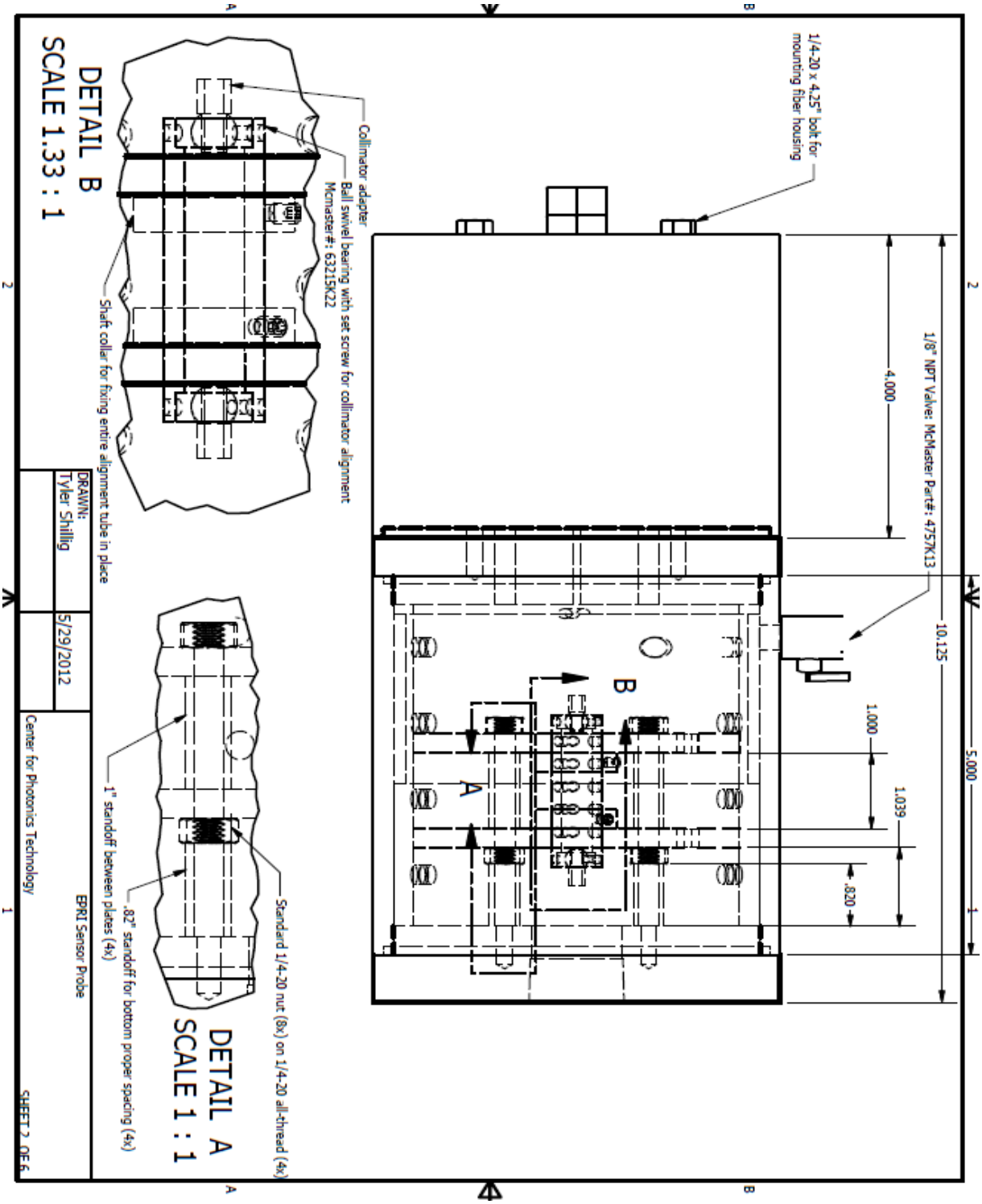

Sensor prototype drawing

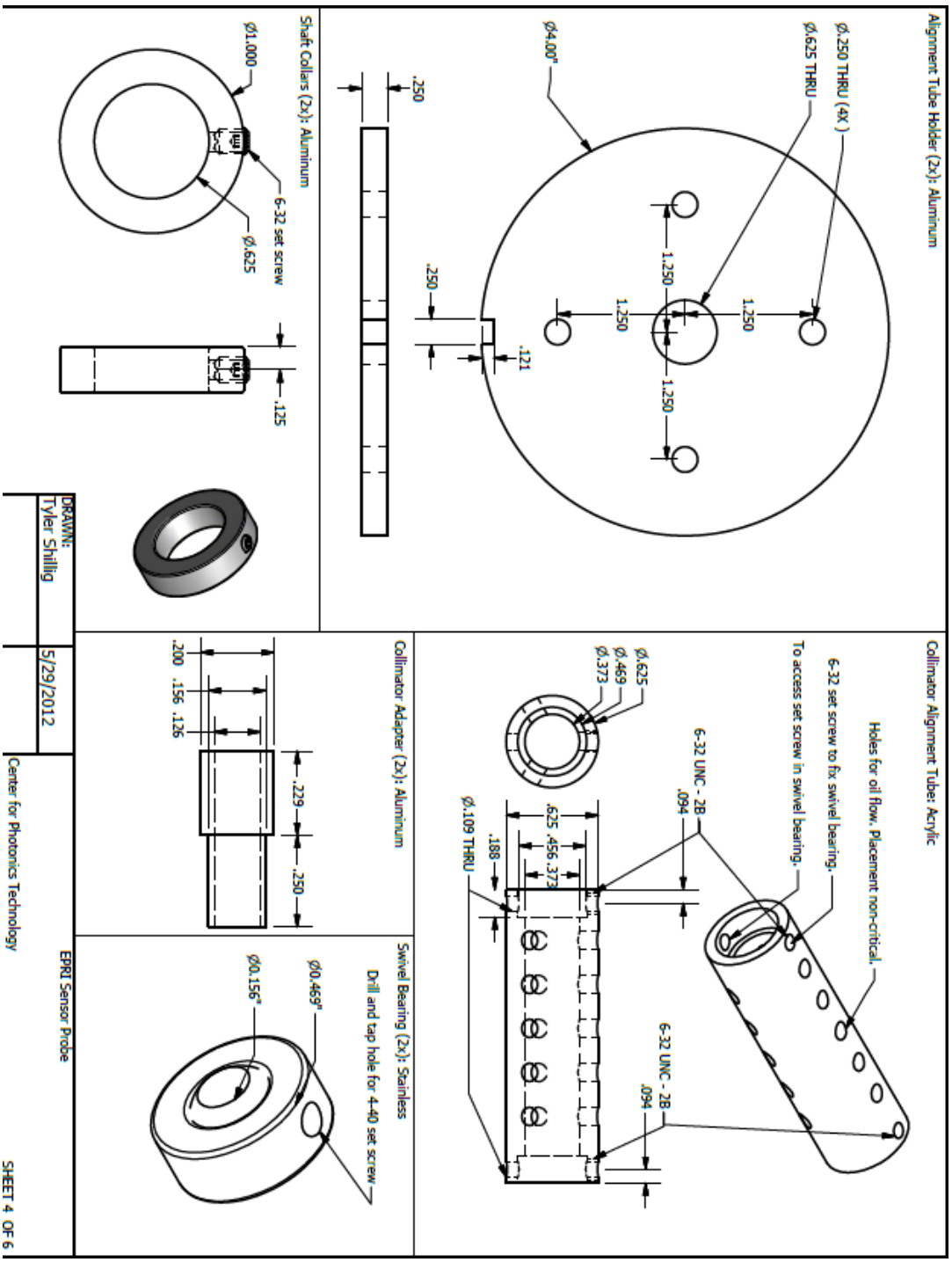

Acetylene Sensor Probe Design

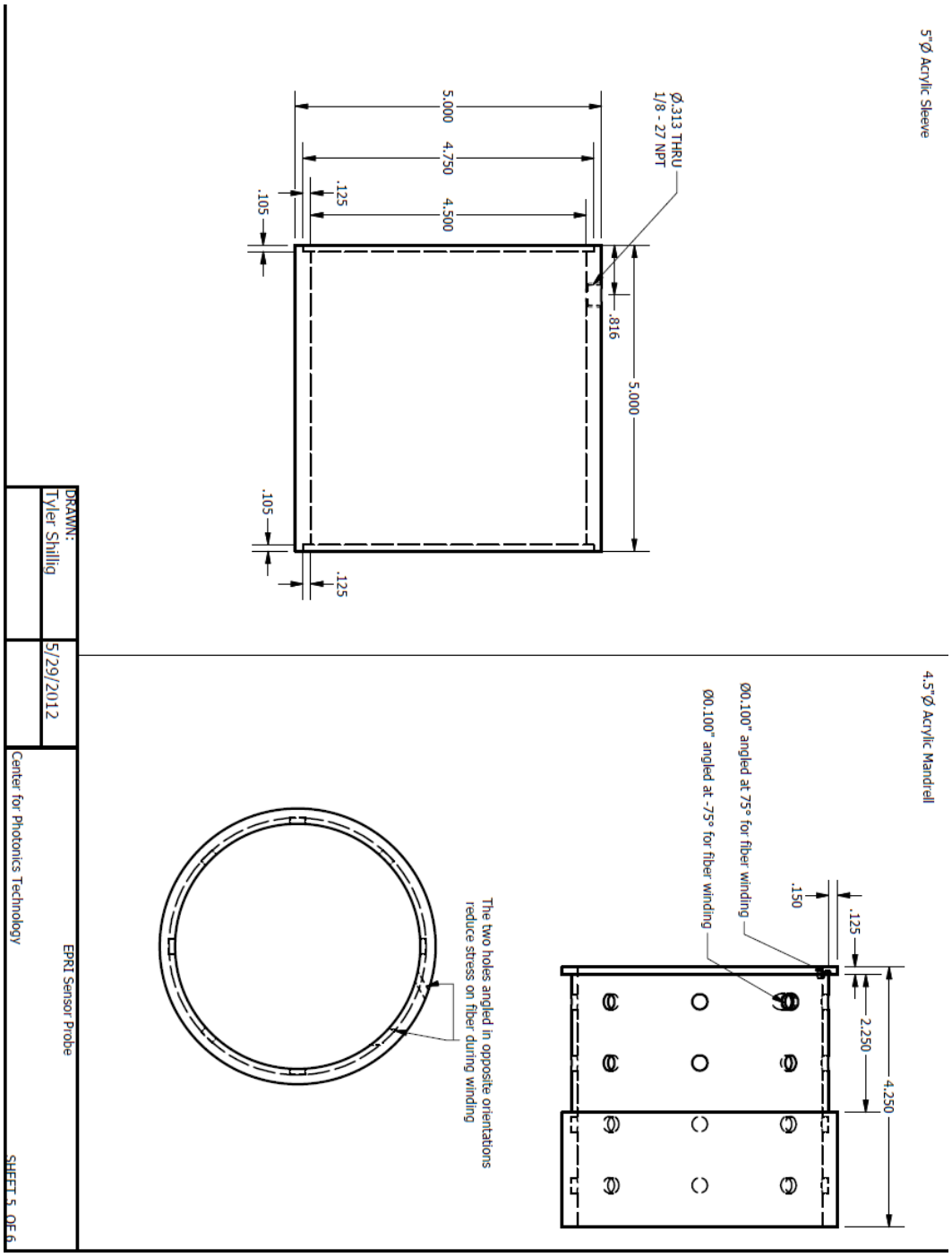

Hydrogen Mandrel Design

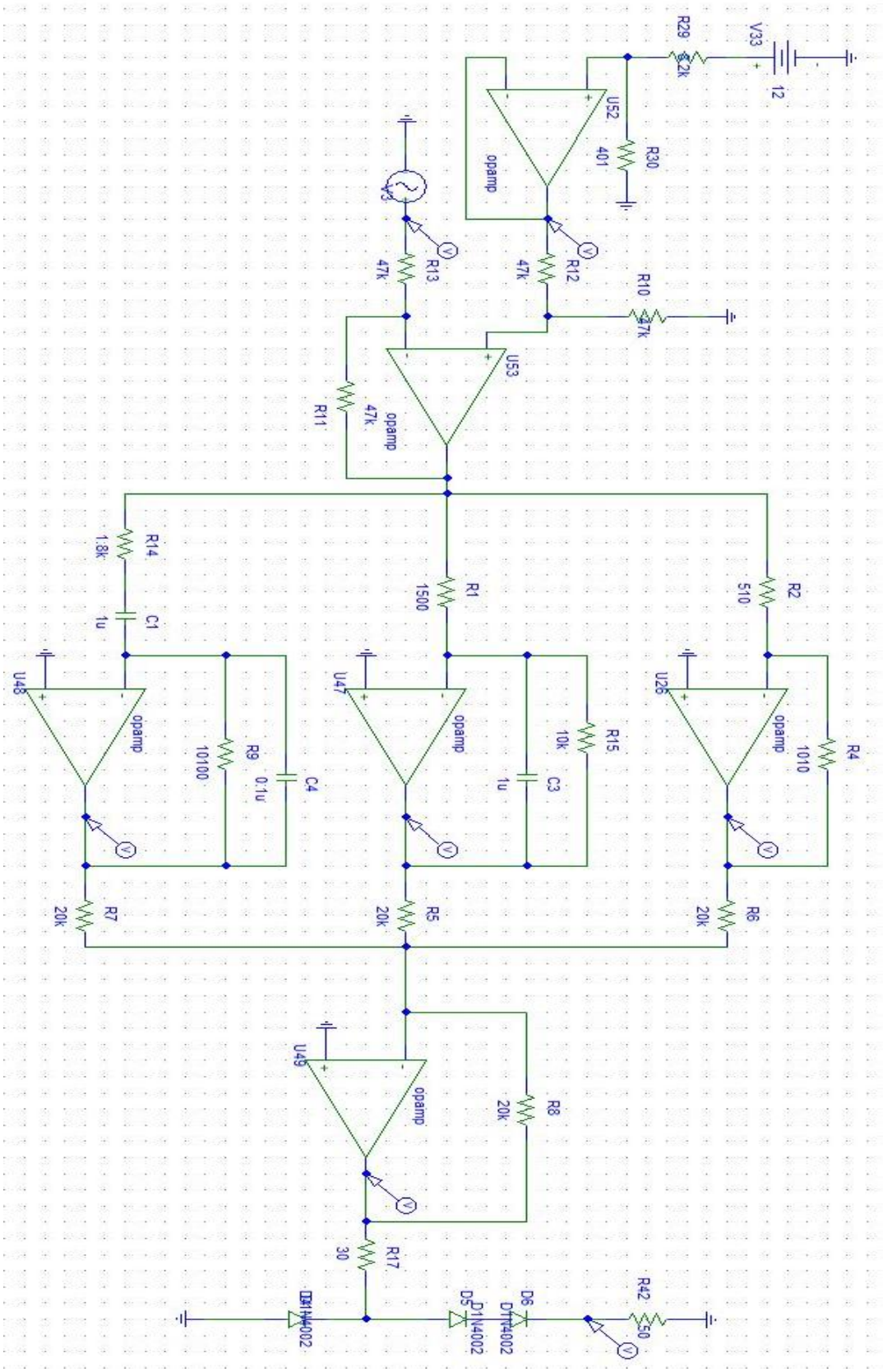

Analog PID design

Microcontroller PID Code for Texas Instruments MP4431

Main.c - Initialization and PID call

```
#pragma config WDTEN = OFF
#pragma config MCLRE = OFF
#pragma config LVP = OFF
#pragma config OSC = IRCIO
#pragma config SSPMX = RD1 // enables SPI on PORTD

#include <p18f4431.h> /* header file for PIC18F4431*/
#include "SPICom.h"

#define OSCOPE LATCbits.LATC0

void main(void); /* main code */
void init(void); /* Intialisition of the PIC */
void highint(void); /* Interupt Service Routine */
float PIDcal(float,float); // PID Routine
static short int IntCount=0;
int ADin;
float Vin=0,C_PID_Out=0,C_DACin=0,ADref=0,C_PIDcor=0;

#pragma interrupt highint
void highint (void){
        if (PIR1bits.TMR1IF==1){
                PIR1bits.TMR1IF=0; /*clear interrupt flags */
                PIE1bits.TMR1IE=0; // Disable timer1 interrupt
                PIE1bits.ADIE=0;      // Disable A/D interrupt

//              IntCount++;
                if(IntCount >=3){
                        IntCount=0;
                        ADCON0bits.GO = 1; // Enable ADC read
                }
                PIE1bits.TMR1IE = 1; // Enable timer1 interrupt
                PIE1bits.ADIE=1;      // Enable A/D interrupt
        }
        if (PIR1bits.ADIF == 1){
                PIR1bits.ADIF = 0; //reset the AD interrupt
                PIE1bits.TMR1IE=0; //Disable timer1 interrupt
                PIE1bits.ADIE=0; //Disable A/D interrupt

                ADin = (ADRESH); // Read from ADC and convert to float
```

```
                ADin = (ADin << 2) + (ADRESL >> 6);
                Vin = (float)ADin*(ADref)/(1024);

                C_PID_Out = PIDcal(0.560,Vin); //Call PID(setpoint,actual)
                C_PIDcor = Vin+C_PID_Out;
                C_DACin = C_PIDcor*2.6+1.9; //Offset correction for I/O
                if(C_DACin < 1.90) C_DACin = 1.90; // Min Amp input = 1 V
                VinDACa(C_DACin,Vref);

                ADCON0bits.GO = 1; // Enable ADC read
                PIE1bits.TMR1IE = 1; // Enable timer1 interrupt
                PIE1bits.ADIE=1; // Enable A/D interrupt
        }
}

#pragma code highvector=0x0008
void highvector(void){
        _asm goto highint _endasm
 }

#pragma code
void main(){
        init(); // Initialize PIC
        Vref = 5;
        ADref = 1.225; // Calibrated to FLUKE 179 Multimeter
        VinDACa(2.00,Vref);
        ADCON0bits.GO = 1;
        while(1){ /*Continous Loop*/
        }
}

void init(){
        // Oscillator Setup
        OSCCON = 0x70; // Oscillator set to 8 MHz
        OSCTUNE = 0x3F; // Tune for max frequency

        /* Interrupt Setup */
        INTCON = 0x00; /* Clear Registers */
        PIR1 = 0x00;
        PIE1 = 0x00;
        TMR1L = 0x00;
        TMR1H = 0x00;
        T1CON = 0x00;
        RCON = 0x00;

        /* Interrupt and Timer Configuration */
```

```
        RCONbits.IPEN = 1; /* Set Priorities */
        INTCONbits.GIEL = 0; /* disable low priority interrupts */
        INTCONbits.GIEH = 1; /* enable high priority interrupts */
        T1CONbits.RD16 = 1; /* Enable 16bit read/write of timer. */
        T1CONbits.T1CKPS1 = 0; /* Set Prescaler 1:1 */
        T1CONbits.T1CKPS0 = 0;
        T1CONbits.TMR1CS = 0; /* Increment every instructrion cycle */
        IPR1bits.TMR1IP = 1; /* Make high priority interrupt */
        T1CONbits.TMR1ON = 1; /* Enable the timer */
        PIE1bits.TMR1IE = 1; /* Enable timer1 interrupt */
        PIE1bits.ADIE=1;      // Enable A/D interrupt

        /* Load timer for interupt every 0.9525 mseconds */
        TMR1H = 0xC0; /* Load timer1 higher byte */
        TMR1L = 0x1D; /* Load timer1 lower byte */

        /* Port Set Up*/
        TRISA = 0xFF;/* Set portA for analog input */
        TRISB = 0x00;/* Set all other pins for ouputs. */
        TRISC = 0x00;
        TRISD = 0x00;
        TRISE = 0x00;

        // ADC Init, Measurements on Ch B (AN 1)
        ADCON1 = 0b01000000; //External Vref+
        ADCON2 = 0b00110000; //Right Justified,12 Tad,Fosc/2
        ADCON3 = 0b11000000; //Unimplemented
        ADCHS = 0b00000000;
        ANSEL0 = 0b00000010; // Ch B input
        ANSEL1 = 0b00000000;
        ADCON0 = 0b00000101; //Single Shot,Single Ch B,Go off,ADOn

        // SPI Init
        SPI_Init();

        OSCOPE=0;
}
```

CPID.c - PID Algorithm

```
#include <p18f4431.h>

//Define parameter
#define epsilon 0.0001 //0.001
#define dt 0.1 //0.01          //loop time
#define MAX  5                 //For Current Saturation
#define MIN -5
#define Kp  0.9 // 0.9
#define Ki  0.04 // 0.4
#define Kd  0.005 // 0.005

float PIDcal(float setpoint,float actual_position)
{
        static float pre_error = 0;
        static float integral = 0;
        float error;
        float derivative;
        float output;

        //Caculate P,I,D
        error = setpoint - actual_position;

        //In case of error too small then stop integration
        if((error > epsilon) || (-1*error > epsilon)){
                integral = integral + error*dt;
        }
        derivative = (error - pre_error)/dt;
        output = Kp*error + Ki*integral + Kd*derivative;

        //Saturation Filter
        if(output > MAX){
                output = MAX;
        }
        else if(output < MIN){
                output = MIN;
        }
      //Update error
      pre_error = error;

 return output;}SPICom.c – Interfacing Code from MCU to EOM

#include <delays.h>
#include "SPICom.h"
```

```
void SPI_Init (void){
	TRISDbits.TRISD0 = 0; //pin 19, used for CS on DAC
	TRISDbits.TRISD1 = 0; //SDO - RD1, pin 20
	TRISDbits.TRISD2 = 1; //SDI - RD2, pin 21 (not used)
	TRISDbits.TRISD3 = 0; //SCK - pin23, Set Master Mode for clock

	PIE1bits.SSPIE = 0;    //interrupt enable (disabled)
	PIR1bits.SSPIF = 0;    //interrupt flag (disabled)
	IPR1bits.SSPIP = 0; //SSPIP: Synchronous Serial Port Interrupt Priority bit (1 = high)

	DAC_CS = 1; // CS pin must be pulled low to enable transfer

	SSPCON=0x20; //(def: 0x20) Enable, Mode 0 0
	SSPSTAT=0x40; //(def: 0x40) Master, Mode 0 0, Fosc/4
}

void SPI_Close(void){
	PIE1bits.SSPIE = 0; // Disable interrupts
	SSPCONbits.SSPEN = 0; // Disables SPI
}

unsigned char SPI_Write(unsigned char out){
	SSPBUF = out;
	while(!SSPSTATbits.BF);
}

unsigned char SPI_Read_Byte(void){
	return SSPBUF;
}

void VinDACa(unsigned float Vout,static float Vref){ // Load in value in Volts
	// Vout=((Vref*[binary code]*Gain)/4095
	unsigned short int code;

	if(Vout < 0) Vout = 0; // Set limit of DAC
	else if (Vout > Vref) Vout = Vref;

	code =(Vout*819); //(Vout*4095)/(Vref*1);
	LoadDAC(code,0);
}

void VinDACb(unsigned float Vout,static float Vref){
	// Vout=((Vref*[binary code]*Gain)/4095
	unsigned short int code;

	if(Vout < 0) Vout = 0; // Set limit of DAC
```

```
        else if (Vout > Vref) Vout = Vref;

        code =(Vout*819); //(Vout*4095)/(Vref*1);
        LoadDAC(code,1);
}

void LoadDAC(unsigned short int dac,unsigned short int select){ // loads data to DAC, dac=2
bytes containing data, select chooses DAC (0=A)(1=B)
        if(select==0) dac = dac | 0x3000;  //Insert command DACa, unbuffered, G = 1, output
ON (default 0x3000)
        else if (select==1) dac = dac | 0xB000;  //Insert command DACb, unbuffered, G = 1,
output ON (default 0xB000)
        else return;

        DAC_CS = 1;
        DAC_CS = 0; // pull CS bit low to enable DAC

        SSPBUF = (unsigned char)(dac >> 8);
        while(!SSPSTATbits.BF);
        SSPBUF = (unsigned char)(dac & 0x00ff);
        while(!SSPSTATbits.BF);

        DAC_CS = 1; // pull CS bit high to output DAC
}
```

SPI.h – Routine Call for SPI.C

```
#include <p18f4431.h>

#define DAC_CS LATDbits.LATD0 // set high to write to DAC, low to get output
#define SPI_SDO LATDbits.LATD1
#define SPI_SDI LATDbits.LATD2
#define SPI_SCK LATDbits.LATD3

void SPI_Init (void);
void SPI_Close(void);
void VinDACa(unsigned float Vout,static float Vref);
void VinDACb(unsigned float Vout,static float Vref);
void LoadDAC(unsigned short int dac,unsigned short int select);
unsigned char SPI_Write(unsigned char out);
unsigned char SPI_Read_Byte(void);
static float Vref;
```